Vortex matter freezing in $Bi_2Sr_2CaCu_2O_8$ samples with a very dense distribution of columnar defects

N. R. Cejas Bolecek,[1] A. B. Kolton,[2] M. Konczykowski,[3] H. Pastoriza,[4] D. Domínguez,[2] and Y. Fasano[4]

[1] *Low Temperature Lab, Centro Atómico Bariloche & Instituto Balseiro, Bariloche, Argentina*
[2] *Solid State Theory Group, Centro Atómico Bariloche & Instituto Balseiro, Bariloche, Argentina*
[3] *Laboratoire des Solides Irradiés, CNRS-UMR 7642 & CEA-DSM-IRAMIS, Ecole Polytechnique, F 91128 PALAISEAU, France*
[4] *Laboratorio de Bajas Temperaturas, Centro Atómico Bariloche & Instituto Balseiro, Bariloche, Argentina*

(Dated: June 22, 2015)

We study dynamically-frozen vortex configurations in heavy-ion irradiated $Bi_2Sr_2CaCu_2O_8$ samples with a dense distribution of columnar defects corresponding to a matching field $B_\Phi = 5\,\mathrm{kG}$. We analyze magnetic decoration images obtained at diluted vortex densities, $B \sim 10^{-2}B_\Phi$, frozen at a temperature T_{freez} between the onset of irreversible magnetic behavior and the decoration temperature of 4.2 K. We find amorphous configurations with liquid-like correlations and Gaussian distributions of the components of the vortex-defect forces. Assuming strongly localized vortices we propose a model that shows that the observed translational order is fairly consistent with a relaxation dynamics dominated by double-kink excitations near the freezing temperature. We predict a T_{freez} of the same order but smaller than the irreversibility and the first-order transition temperatures. We argue that the low-field vortex structures nucleated in a dense distribution of columnar defects correspond to a typical configuration of a non-entangled liquid with strongly reduced mobility rather than to a metastable glassy phase with divergent activation barriers.

PACS numbers: 74.25.Uv,74.25.Ha,74.25.Dw

I. INTRODUCTION

Understanding the impact of different types of disorder on elastic systems is important both for fundamental and applied condensed matter physics. This issue is relevant for a variety of experimental systems ranging from vortex lattices[1,2] and flux-penetration in superconductors[3], charge-density waves[4], domain walls in ferromagnetic [5,6] or ferroelectric [7] materials, contact lines of liquids [8], to crack propagation in solids.[9] All these systems share a common physics arising from the competition between elasticity and disorder. This balance yields a rich behavior with universal features observable in static and dynamic properties at a coarse-grained scale such as glassy phases, metastability, slow relaxation and pinning. Vortices nucleated in high-temperature superconducting samples are one of the paradigmatic systems to study this phenomena since the relevant energies are easily tuned by changing temperature, magnetic field, and by introducing different types of disorder. In addition, direct imaging techniques[2,10,11] allow visualizing the resulting spatial structures and analyzing the impact of disorder on the otherwise perfect equilibrium Abrikosov lattice.

Inferring the effect of disorder from magnetic decoration snapshots[12,13] of quenched vortex structures with a large number of vortices has become a promising avenue to perform these studies.[14–19] This technique provides a two-dimensional top view at the sample surface of the three-dimensional vortex lattice frozen at a temperature T_{freez}. In order to move forward on the quantification of the impact of disorder in the vortex structure from these images, better understanding or modelling of the vortex dynamics during the cooling process is necessary. In field-cooling experiments, an initial high-temperature vortex state is driven into an almost-frozen configuration at some unknown intermediate temperature, further stabilized at the lower temperatures at which magnetic decorations are performed.[12,13] Having a quantitative understanding of this process is in general a difficult task due to the non-equilibrium and non-stationary nature of the three-dimensional thermally-activated vortex dynamics over pinning barriers. Therefore, in order to undergo this study is desirable to find a convenient experimental situation in which the vortex dynamics modelling could be simplified. The case of high-temperature superconductors with artificially-introduced strong pinning centers such as columnar defects (CD) offers such a possibility, particularly for a high density of pins. Vortices are then expected to become individually localized at CD and the quenching of their thermally-activated motion can be modelled in terms of well known excitations.[1]

High-T_c superconductors with CD introduced by heavy-ion irradiation were largely studied during the last two decades leading to an accurate knowledge of the effect of the pinning landscape on the critical current. [20–22] The interaction of individual vortices with single pins was studied theoretically [23–26] as well as experimentally.[27] The spatial distribution of columns resulting from heavy-ion irradiation follows a random Poisson-like statistics.[28,29] The equivalent method of generating individual defects lead to suppose that all columnar tracks have a nearly equal magnitude of bare pinning energy U_0. In the case of cuprate high-T_c superconductors the magnitude of this pinning energy outweighs that of any other type of cristalline disorder provided $U_0 \propto 1/\xi^2$.[1] Since distributions of columnar tracks with different density

can be generated just by tuning the heavy-ions irradiation dose, CD in cuprates are therefore a model system for studying vortex distributions in the presence of strong correlated disorder.

In this work we study the structural properties of vortex matter nucleated in $Bi_2Sr_2CaCu_2O_8$ samples with a very dense distribution of CD. The structural properties of this system were previously studied for lower doses of CD than the one we report here.[30–37] In the case of a large ratio of CD to vortices, $n_{\rm CD}/n_{\rm v} = B_\Phi/B$, with $B_\Phi = n_{\rm CD}\Phi_0$ the matching field, a complete destruction of the positional and orientational order of the vortex structure is reported. [30] However, for CD densities two orders of magnitude smaller, the short-range order of the vortex structure is recovered[31] and a polycristalline structure is observed. [32–37] Therefore, at low densities of CD the inter-vortex repulsion remains important even in the presence of such strong pinning centers. Theoretical studies suggested that even in the case of a high-density of CD the subset of occupied defects is strongly affected by the inter-vortex repulsion.[29] Indeed, a close inspection to the pair correlation function for samples with a large density of CD reveals that the structure of the vortex ensemble is that of a disordered glass with only a well defined first-neighbors distance. It is important to point out that the imaged vortex states are not at equilibrium at the observation (decoration) temperature. These configurations correspond to the state frozen at a certain temperature $T_{\rm freez}$ slightly below the irreversibility temperature at which vortex mobility is strongly reduced by the effect of bulk pinning.[10,38]

II. EXPERIMENTAL

The single-crystal of optimally-doped $Bi_2Sr_2CaCu_2O_8$ studied here was grown by the travelling-floating-zone method[39] and irradiated by 6 GeV Pb-ions at GANIL. The irradiation dose was chosen in order to obtain a density of 2.42×10^{10} CD per square centimeter corresponding to a matching field of $B_\Phi = 5\,$kG. Every single ion impact creates an amorphous columnar track with a radius $r_{\rm r} \sim 3.5\,$nm, roughly parallel to the c-axis through the entire sample thickness. This gives a bare-pinning energy per unit length per CD at zero temperature of $U_0 = \varepsilon_0 \ln(r_{\rm r}/\sqrt{2}\xi(0)) \sim 6\varepsilon_0(0) \sim 4 \times 10^{-6}\,$erg/cm.

The studied crystal was characterized by means of differential magneto-optics,[14,40] local Hall-probe magnetometry,[41] and magnetic decoration[2] techniques. The sample has a critical temperature $T_{\rm c} = 86.7\,$K, in-plane dimensions of $400 \times 200\,\mu$m^2, and thickness of some tens of microns. Magneto-optical imaging shows rather homogeneous flux penetration into the crystals and does not reveal any noticeable large-scale surface or bulk defect.

The H-T phase diagram of $Bi_2Sr_2CaCu_2O_8$ vortex matter with such a dense distribution of CD was obtained by means of local Hall-probe magnetometry up to 10000 G. These measurements were performed using microfabricated 2D-electron-gas Hall-magnetometers that locally probe the sample stray field.[41] The low-field data ($H < 200\,$G) were obtained with an array of 10 sensors linearly spaced every $20\,\mu$m, each individual sensor with a $5\times5\,\mu$m^2 active surface. The high-field data ($H > 200\,$G) were measured with a single $10 \times 10\,\mu$m^2 active-surface sensor. In all cases, the Hall sensors were placed at the center of the sample.

Magnetic transmittivity measurements were performed by applying an ac excitation field $H_{\rm ac}$ parallel to a dc field H. The Hall data presented here were obtained with an excitation field of 1.2 Oe rms and 11 Hz. The current applied to the Hall sensors is in the range of 50 to $100\,\mu$A. A digital-signal-processing lock-in technique is used to simultaneously measure the in- and out-of-phase components of the fundamental and the third-harmonic signals of the Hall voltage. The fundamental signal was used to obtain the thermodynamic first-order transition line,[42,43] $H_{\rm FOT}(T)$, from transmittivity measurements. [44] The third-harmonic signal yields information on the onset of irreversible magnetic behavior, namely the irreversibility line $H_{\rm irr}(T)$.[44]

The structural properties of vortex matter nucleated on the same crystal were directly imaged by means of magnetic decoration experiments. [2] This study was limited to magnetic fields below 80 Oe since for this sample the technique looses single-vortex resolution at larger vortex densities.The sample was field-cooled from $T > T_{\rm c}$ down to 4.2 K in roughly 15 min and magnetic decorations were performed at this base temperature. The vortex structural properties revealed by this technique, at the lengthscales of the lattice parameter, correspond to those frozen at the temperature at which vortex mobility gets reduced by the effect of the pinning potential.[38] We will discuss later the relation between this freezing temperature $T_{\rm freez}$ and the lines presented in the phase diagram explored by means of Hall magnetometry.

III. EXPERIMENTAL RESULTS

A. Vortex phase diagram

Figure 1 (b) shows the vortex phase diagram of $Bi_2Sr_2CaCu_2O_8$ vortex matter nucleated in samples with a CD density of $B_\Phi = 5\,$kG. The first-order, $H_{\rm FOT}$, and irreversibility, $H_{\rm irr}$, lines are obtained from measuring the sample magnetic response by means of ac Hall magnetometry.[44] Figure 1 (a) shows the temperature evolution of normalized first and third-harmonic signals in the low-field range up to 140 Oe. The transmittivity T' is obtained from the in-phase component of the first-harmonic signal, B', considering that $T' = [B'(T) - B'(T \ll T_{\rm c})]/[B'(T > T_{\rm c}) - B'(T \ll T_{\rm c})]$[45]. This magnitude is highly-sensitive to discontinuities in the local induction as for example the one entailed at the $H_{\rm FOT}$ transition towards a vortex liquid[42,43] or a decoupled gas of pancakes[46] at high temperatures. The normalized modulus

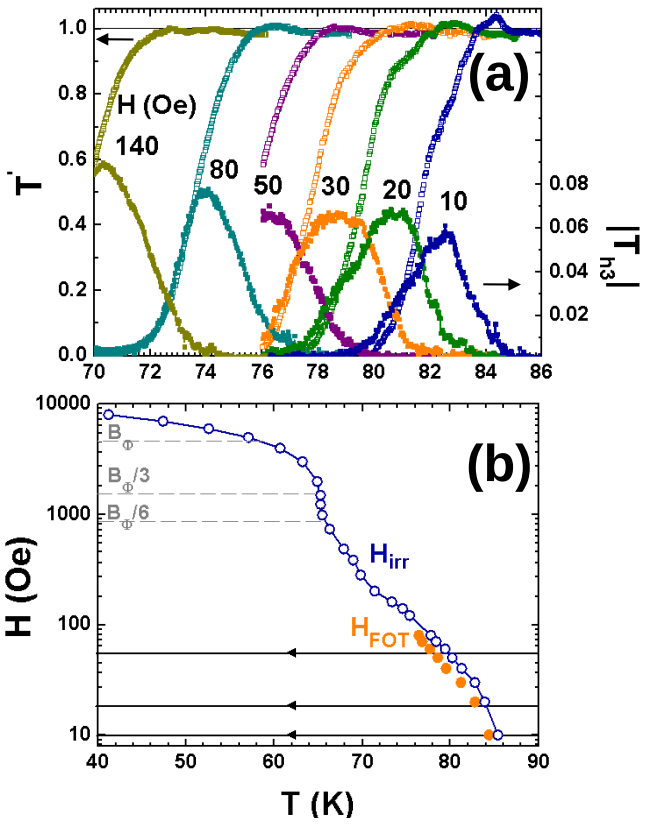

Figure 1: Vortex phase diagram for $Bi_2Sr_2CaCu_2O_8$ with a dense distribution of CD with $B_\Phi = 5\,\mathrm{kG}$. (a) Temperature-dependence of the transmittivity, T', and modulus of the third-harmonic response, $|\,T_{h3}\,|$, at low applied fields. The ac ripple field is collinear to the dc field $H \parallel c$. (b) Irreversibility, $H_{\rm irr}$, and first-order, $H_{\rm FOT}$, transition lines obtained from T' and $|\,T_{h3}\,|$ data as indicated in the text. Full lines indicate the field-cooling processes followed during the magnetic decoration experiments.

of the third-harmonic signal $|\,T_{h3}\,| = |\,B^{AC}_{h3}\,|\,/[B'(T > T_c) - B'(T \ll T_c)]$ becomes non-negligible at the onset of non-linear response arising from irreversible magnetic properties.

The high-temperature $H_{\rm FOT}$ transition is detected in ac transmittivity measurements as a frequency-independent so-called paramagnetic peak that develops in T' at the same H as the jump in local induction detected in dc hysteresis loops.[44,47] The paramagnetic peak is equivalently observed in T' versus temperature curves, see Fig. 1 (a). For a given field, the FOT temperature is typically considered as that where the maximum is detected.[47] For the studied $B_\Phi = 5\,\mathrm{kG}$ sample the paramagnetic peak is clearly observed in T' curves up to 80 Oe. The peak shifts towards lower temperatures on increasing field. On cooling at higher fields, shielding currents develop in the sample prior to the development of the paramagnetic peak fainting its detection.

The irreversibility line is identified from the onset of the third-harmonic signal on cooling. The detection of this onset is frequency-dependent with $T_{\rm irr}$ moving to larger fields on increasing frequency. [48] Figure 1 (a) shows $|\,T_{h3}\,|$ curves as a function of temperature for a ripple field of 11 Hz. In the range $H < B_\Phi/6$, this onset monotonically shifts towards lower temperatures on increasing field. At intermediate fields, $B_\Phi/6 < H < B_\Phi/3$, the onset of irreversibility is almost field-independent as observed in the vortex phase diagram of Fig. 1 (b). At larger fields, a monotonous increase of $H_{\rm irr}$ with reducing field is again observed. This field-evolution of the irreversibility line is common to $Bi_2Sr_2CaCu_2O_8$ samples with high-densities of CD and has origin in the three different regimes for the occupation of columnar defects with vortices discussed in Refs. 49,50.

Figure 1(b) show black lines that indicate the H-T paths followed during the field-cooling magnetic decoration experiments. For all the imaged vortex structures the system undergoes a first-order transition. The $H_{\rm FOT}$ line for this sample is located at lower temperatures than the irreversibility line, $T_{\rm FOT} \sim 0.98 T_{\rm irr}$. This separation between both lines, although of lesser intensity, was also reported in pristine $Bi_2Sr_2CaCu_2O_8$ samples.[48] Therefore, at finite frequencies there is a narrow phase-region with non-linear vortex dynamics at fields exceeding $H_{\rm FOT}$[51].

B. Structural properties of the frozen vortex matter

Figure 2 shows snapshots of the vortex structure obtained in field-cooling magnetic decoration experiments at applied fields of 10, 20 and 60 Oe. Due to the finite magnetization of these samples with pinning enhanced by CD, the local induction measured from the vortex density is smaller than the applied field, $B = 9$, 18.8, and 59.4 G, respectively. In this field range vortices are extremely diluted with respect to the random distribution of CD, every vortex unit cell spanning a spatial region having between 80 (60 Oe) and 500 (10 Oe) defects. In this limit, one can expect that the vortex structure presents similar topological order than in the case of pristine samples with a dense distribution of point pinning centers. Strikingly, the observed vortex structures are amorphous, irrespective of the vortex density within the studied range. These results follow the same trend than magnetic decoration data on samples with a less-dense distribution of CD ($B_\Phi = 3.5\,\mathrm{kG}$) were a complete destruction of translational order was reported.[30]

The Delaunay triangulations of the right panels of Fig. 2, indicating the first-neighbors for each vortex, reveal that the structures have the non-sixfold coordination typical of an amorphous. The ring-like patterns of the Fourier transform of vortex positions shown in the insert confirm the lack of short-range positional and orientational orders. Indeed, the pair correlation functions $g(r)$ of Fig. 3(a) show only one distinguishable peak at the first-neighbors distance, irrespective of significantly in-

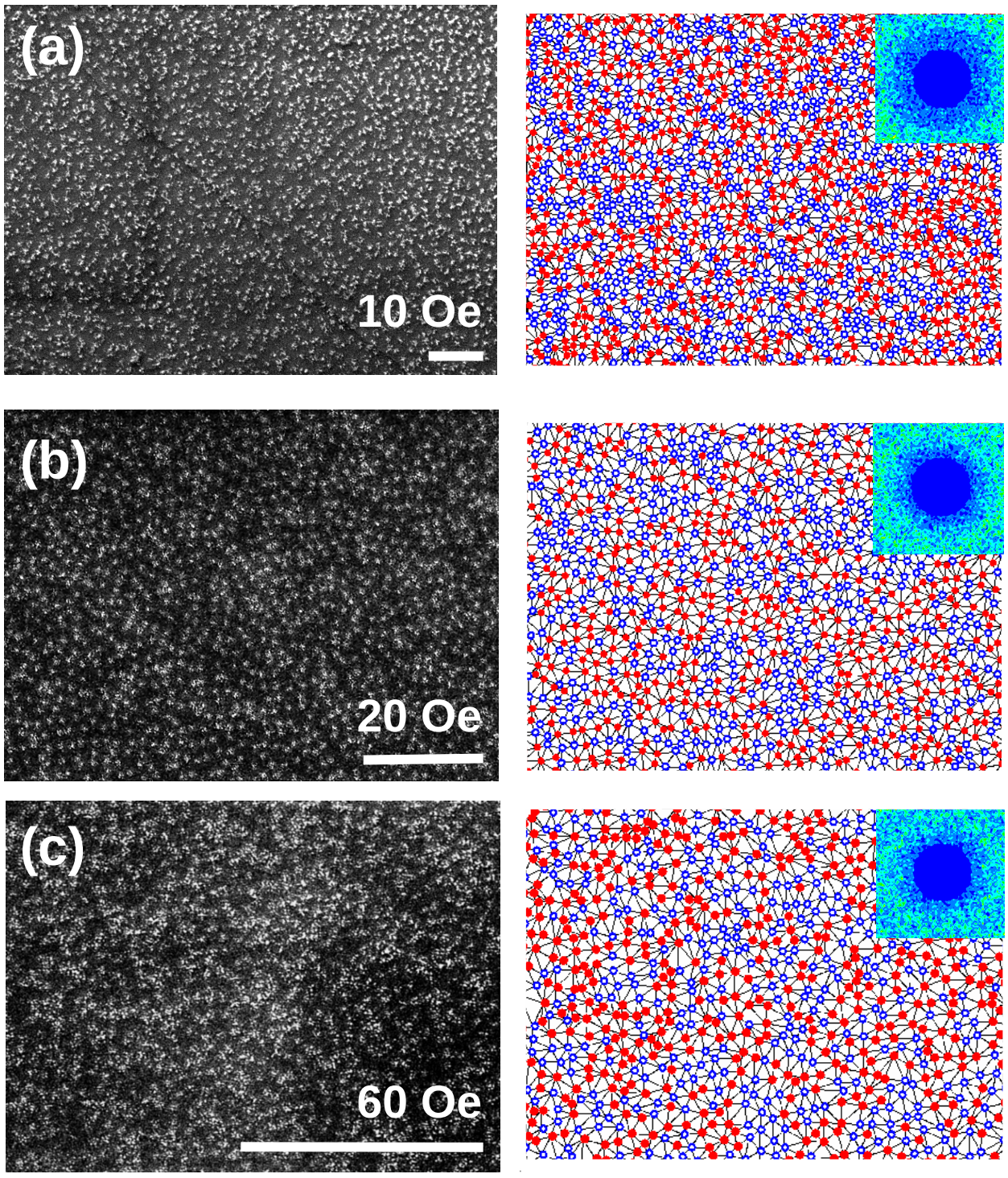

Figure 2: Vortex structure in $Bi_2Sr_2CaCu_2O_8$ samples with a CD density corresponding to $B_\Phi = 5\,\mathrm{kG}$ for applied fields of (a) 10, (b) 20 and (c) 60 Oe. Left panels: Magnetic decoration images of the vortex structure taken at 4.2 K after field-cooling from the liquid vortex phase. The white bars correspond to 10 μm. Right panels: Delaunay triangulations indicating first-neighbors and sixfold (blue) and non-sixfold (red) coordinated vortices. The inserts show the Fourier transform of the vortex positions.

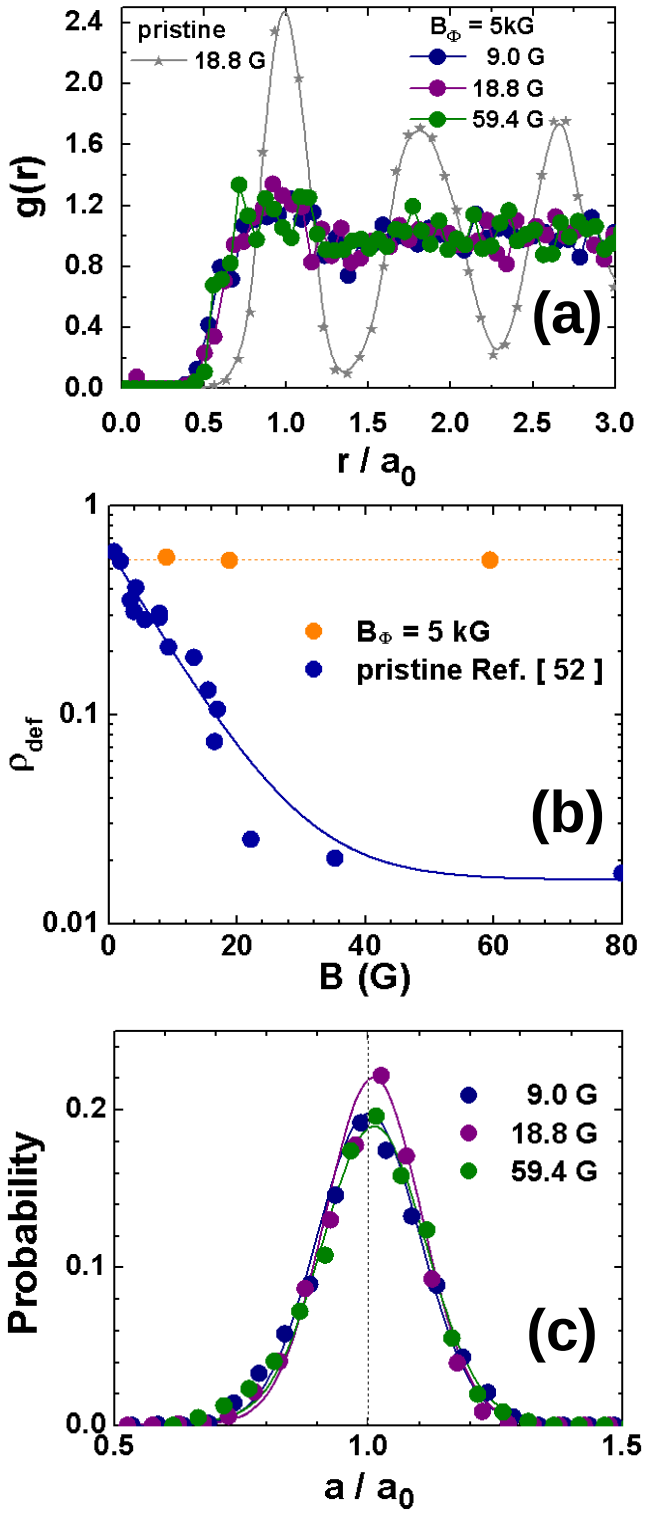

Figure 3: Structural properties of $Bi_2Sr_2CaCu_2O_8$ vortex matter nucleated in samples with a dense distribution of CD corresponding to $B_\Phi = 5\,\mathrm{kG}$. (a) Pair-correlation function for the vortex structures nucleated at several fields (circles). For comparison, we show the results in a pristine sample at 18.8 G. (b) Field-evolution of the density of non-sixfold coordinated vortices obtained from the images of Fig. 2 as compared to the case of vortex matter nucleated in pristine samples. Lines are guides to the eye. (c) Distribution of first-neighbors distances, a, normalized by the average lattice spacing a_0 (points). The full lines are fits to the data with Gaussian functions.

creasing the inter-vortex interaction. This contrasts with the $g(r)$ obtained for pristine samples that present peaks up to several lattice spacings (see the curve with stars in Fig. 3 (a)). The sixfold coordinated vortices (blue) form very small crystallites containing at best 10 vortices. The density of these vortices is always below 40 % and does not vary significantly on increasing field, see Fig. 3 (b). Quantitatively similar results are obtained for samples with a much more diluted distribution of CD when $\sqrt{B/B_\Phi} < 1.1$[34]. Figure 3 (b) also shows that the density of vortices belonging to topological defects, ρ_{def}, is significantly larger in samples with a dense distribution of CD than in the case of vortex matter nucleated in pristine $Bi_2Sr_2CaCu_2O_8$ samples.[52] However, since magnetic decoration images are snapshots of the vortex structure, distinguishing between an amorphous glassy and a liquid vortex phase is not possible with this technique.

Similar amorphous structures were recently reported for the strongly-pinned vortex matter in pnictide $BaFe_2(As_{1-x}P_x)_2$ and $Ba(Fe_{1-x}Co_x)_2As_2$ samples, [14,16] presenting significant vortex-density fluctuations were reported, more pronounced in the Co-doped system. The disorder of the vortex structure was quantitatively ascribed to the strong inhomogeneous disorder present in the samples.[14] On the contrary, in the $Bi_2Sr_2CaCu_2O_8$ samples studied here, vortex density fluctuations are not very strong, as observed in the histograms of a/a_0 shown in Fig. 3 (c). These histograms are well fitted by a symmetric Gaussian distribution with full-width at half-maximum ranging 23-20 %. The data are normalized by the lattice parameter $a_0 = 1.075\sqrt{\Phi_0/B}$, with B obtained from the vortex density measured in magnetic decoration images.

In the field-cooling magnetic decoration experiments performed here, vortex matter is nucleated in the high-temperature liquid phase and vortices have a high mobility since the decoupled pancakes present a low shear viscosity.[46] On cooling, at T_{freez} vortex mobility gets reduced by the effect of the CD pinning potential and the vortex structure gets frozen, at lengthscales of the lattice parameter a_0, in one of the many available metastable states. On further cooling to lower temperatures, vortices accommodate in order to profit from the pinning potential in all their length at lengthscales of the order of coherence length, $\xi \ll a_0$, a lengthscale that can not be resolved by means of magnetic decoration. As a consequence, the structural properties of vortex matter revealed by magnetic decorations at 4.2 K correspond to those of the structure frozen at T_{freez}. Therefore this is the temperature that has to be considered in order to evaluate elastic and electromagnetic properties of vortex matter observed by means of magnetic decoration.

As usually considered in the literature[10,38], it is reasonable to assume that $T_{\mathrm{freez}} \sim T_{\mathrm{irr}}$ since at this last temperature pinning becomes dominant over the other energy scales. There can be a slight shift between these two temperatures since the T_{irr} determined from ac magnetometry experiments is a frequency-dependent magni-

tude. Nevertheless, for sufficiently low frequency, as in the case of the experiments performed here, $T_{\rm freez} \sim T_{\rm irr}$ is a reasonable approximation. We will discuss on Section VI on the validity of this assumption and its implications.

C. Inter-vortex energy and vortex-defect force distributions

In spite of the absence of important fluctuations in vortex density, the pinning potential generated by a dense distribution of CD produces a strong impact in the lattice structural properties, particularly evident in the spatially inhomogeneous inter-vortex interaction energy. Figure 4 shows the interaction-energy distributions obtained from mapping this energy for the vortex positions of the decoration images of Fig. 2. The interaction energy for a vortex i with its nearest neighbors j located at a distance $\mid r_{\rm ij} \mid$ has a value, per unit length,

$$\varepsilon^{\rm i}_{\rm int} = \sum_{\rm j} 2\varepsilon_0 K_0(\frac{\mid r_{\rm ij} \mid}{\lambda_{\rm ab}}). \qquad (1)$$

K_0 is the zeroth-order modified Bessel function, $\lambda_{\rm ab}$ the in-plane penetration depth and $\varepsilon_0 = (\Phi_0/4\pi\lambda_{\rm ab})^2$ the vortex line-tension. The sum is performed up to a cut-off radius $r_{\rm cut} = 10a_0$ since the interaction energy for every vortex does not change significantly when including terms at larger distances. For every magnetic field, the interaction energy is calculated considering the value of the penetration depth at the temperature at which the vortex structure is frozen that we approximate by $T_{\rm irr}$. We have considered the $\lambda_{\rm ab}(T/T_{\rm c})$ evolution reported in Ref. 22 for pristine $Bi_2Sr_2CaCu_2O_8$ samples and calculated $\lambda_{\rm ab}(T_{\rm irr}/T_{\rm c})$ considering the data of the vortex phase diagram shown in Fig. 1 (b). The penetration depth data of Ref. 22 were measured in pristine samples but $\lambda_{\rm ab}$ for samples with a density of CD of $B_\Phi = 5\,$kG is within 1% this value.[49]

From the interaction energy maps of the vortices of Fig. 2 we obtain the interaction energy distributions of Fig. 4. These distributions are normalized by the line tension ε_0 calculated also considering $\lambda_{\rm ab}(T_{\rm irr})$. This was done with the aim of comparing data at different vortex densities entailing slight changes in $\lambda_{\rm ab}(T_{\rm irr}(B))$. The distributions are asymmetric and do not follow a Gaussian functionality (see full lines in Fig. 4). This contrasts with the a/a_0 histograms and with results found in pnictide samples[14–16]. The energy distributions present a larger statistical weight in the high-energy region, a tendency that is enhanced on increasing vortex density, or equivalently decreasing the number of CD available per vortex. This phenomenology comes from the spatial inhomogeneity induced by the dense CD pinning potential: Although not shown for space reasons, the $\varepsilon_{\rm int}$ maps consist in a rather homogeneous matrix and clusters with larger values. Indeed, vortices with interaction energies

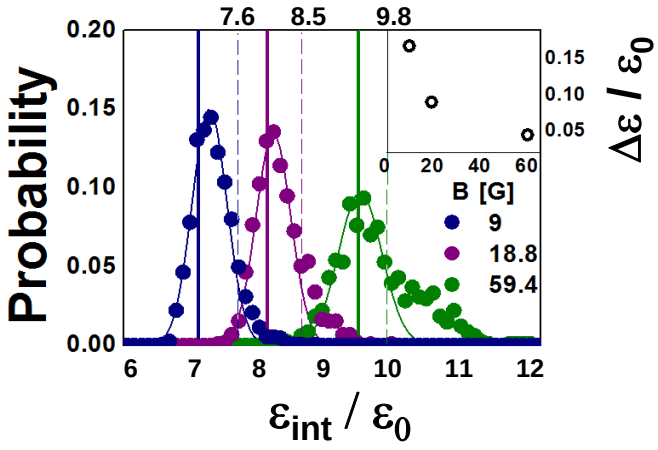

Figure 4: Distributions of normalized individual vortex interaction energies as a function of vortex density for $Bi_2Sr_2CaCu_2O_8$ samples with a dense distribution of CD for the images of Fig. 2. The vertical dotted lines indicate the location of the magnitude of interaction energy corresponding to the mode value plus half-width at half-maximum. The full lines are fits to the data with Gaussian functions. The interaction energy per vortex of the triangular lattice with the same vortex density is shown with vertical full lines for every studied vortex density. Insert: normalized difference between the mode-value of each distribution and the interaction energy value of a perfect hexagonal lattice with similar density.

that exceed the value of the mode of the distribution plus its half-width at half-maximum (values of 7.6, 8.5 and 9.8 indicated in Fig. 4 with dotted lines) are located in vortex clusters with larger interaction energy.

In addition, the maxima of the $\varepsilon_{\rm int}$ distributions are slightly shifted with respect to the interaction energy for a perfect hexagonal structure with the same vortex density (see full vertical lines in the histograms of Fig. 4). As shown in the insert to Fig. 4, the difference between the interaction energy of the perfect lattices and the mode value of the $\varepsilon_{\rm int}$ distributions, $\Delta\varepsilon/\varepsilon_0$, decreases monotonically between 16 and 5% on increasing vortex density in the range between 9 and 59.4 G. This shift was also observed in the case of the pnictide superconductor $Ba(Fe_{1-x}Co_x)_2As_2$, although having a larger value of the order of 70% at $B \sim 9\,$G[14].

Another magnitude that provides important information for understanding the impact of a dense distribution of CD in the vortex structure is the spatial variation of the the inter-vortex repulsive force, $\mathbf{f}_{\rm i}$. Figure 5 shows maps of the magnitude of this force per unit length for each vortex i, $f_{\rm i} \equiv \mid \mathbf{f}_{\rm i} \mid$, computed as the modulus of

$$\mathbf{f}_{\rm i} = \sum_{\rm j} \frac{2\varepsilon_0}{\lambda_{\rm ab}} \frac{\mathbf{r}_{\rm ij}}{\mid \mathbf{r}_{\rm ij} \mid} K_1(\frac{\mid r_{\rm ij} \mid}{\lambda_{\rm ab}}). \qquad (2)$$

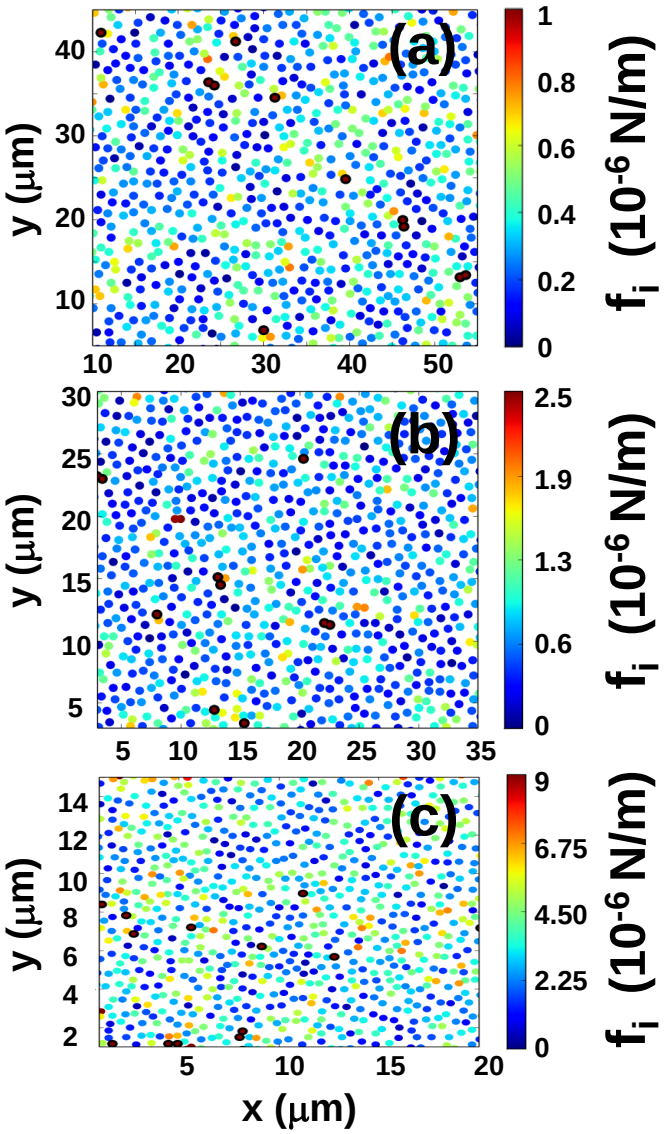

Figure 5: Color-coded maps for the modulus of the inter-vortex repulsive force for vortex densities of (a) 9, (b) 18.8, and (c) 59.4 G corresponding to the decoration images of Fig. 2. Vortices with modulus of the inter-vortex repulsive force larger than the mode value plus half-width at half-maximum are highlighted in black (forces larger than 0.45, 0.9, and $4.5 \times 10^{-6}\,\mathrm{Nm}^{-1}$).

K_1 is the first-order modified Bessel function. We calculated the forces using the same $\lambda_{ab}(T_{irr}(B))$ values, cut-off radius, and excluded edge vortices as in the case of the ε_{int} calculations. Since the vortex structures frozen during the field-cooling processes are close to static metastable equilibrium at $T_{freez}(B)$, non-zero values of f_i can only be ascribed to the force exerted by the CD to individual vortices. Therefore the f_i maps are an accurate estimation of the minimum vortex-defect force at the local scale. These maps are highly inhomogeneous and present clusters with larger inter-vortex force magnitude. The f_i histograms of Fig. 6 (a) show that the mode value monotonically enhances with increasing vortex density. In addition, the distributions are not symmetric and have a larger weight in the high-force part. On increasing vortex density, the f_i distributions broaden significantly and get more asymmetric.

Figure 6 (b) shows the histograms of the x and y components of the interaction force, f_x and f_y. In contrast to the f_i distributions, the force-components distributions are symmetric with respect to zero and their width increases with field. The f_x and f_y distributions are properly fitted with Gaussian functions (see full lines), implying that the individual components of the force varies at random. Therefore, a Rayleigh functionality should be expected for the distribution of the modulus of the force. The fits shown with dotted lines in Fig. 6 (a) and (c) indicate that the distributions of the modulus of the inter-vortex force follow reasonably well this functionality. Therefore the increasing asymmetry of the f_i distributions with B has origin in the increment of the standard deviation of the Gaussian distributions that follow the components of the force.

Finally, Fig. 6 (d) shows that the dispersion obtained from the Rayleigh fits, σ, as well as the maximum value, f_i^{max}, of the f_i distributions increase monotonically with field. The magnitude f_i^{max} corresponds to the maximum value of the defect-vortex pinning force. Considering that the CD pinning force is finite and has a maximum value of $f_c = U_0/r_r$, extrapolating to higher fields the data shown in Fig. 6 (d) yields $f_i^{max} \sim f_c$ at around 4000 G. This suggests a crossover towards vortex configurations with "instersticial vortices", i.e. not located on a CD, at fields $B \sim 0.8 B_\Phi$.

IV. FREEZING DYNAMICS MODEL

In this section we discuss the experimental results in terms of a simple model for the dynamics of freezing of the vortex structure during field-cooling in the presence of the strong disorder associated to a dense distribution of CD. This model allow us to estimate the lifetime of the observed metastable vortex configurations and T_{freez} from characteristic parameters of the system and considering information obtained from magnetic decoration images taken at low fields and 4.2 K (see Fig. 2). We will assume that columnar disorder is strong and dense ($B \ll B_\Phi$) such that, for temperatures of the order of T_{freez}, well defined vortex lines remain most of the time individually pinned in a single columnar defect. Namely, in this model we neglect the effect of point disorder. We will also assume that columnar defects are perfectly parallel to the applied magnetic field.

During the freezing process, pinned vortices form metastable configurations α characterized by the set of occupation numbers of each columnar defect, $\alpha \equiv \{n_k\}$, where $n_k = 1$ if the k-th columnar defect is occupied

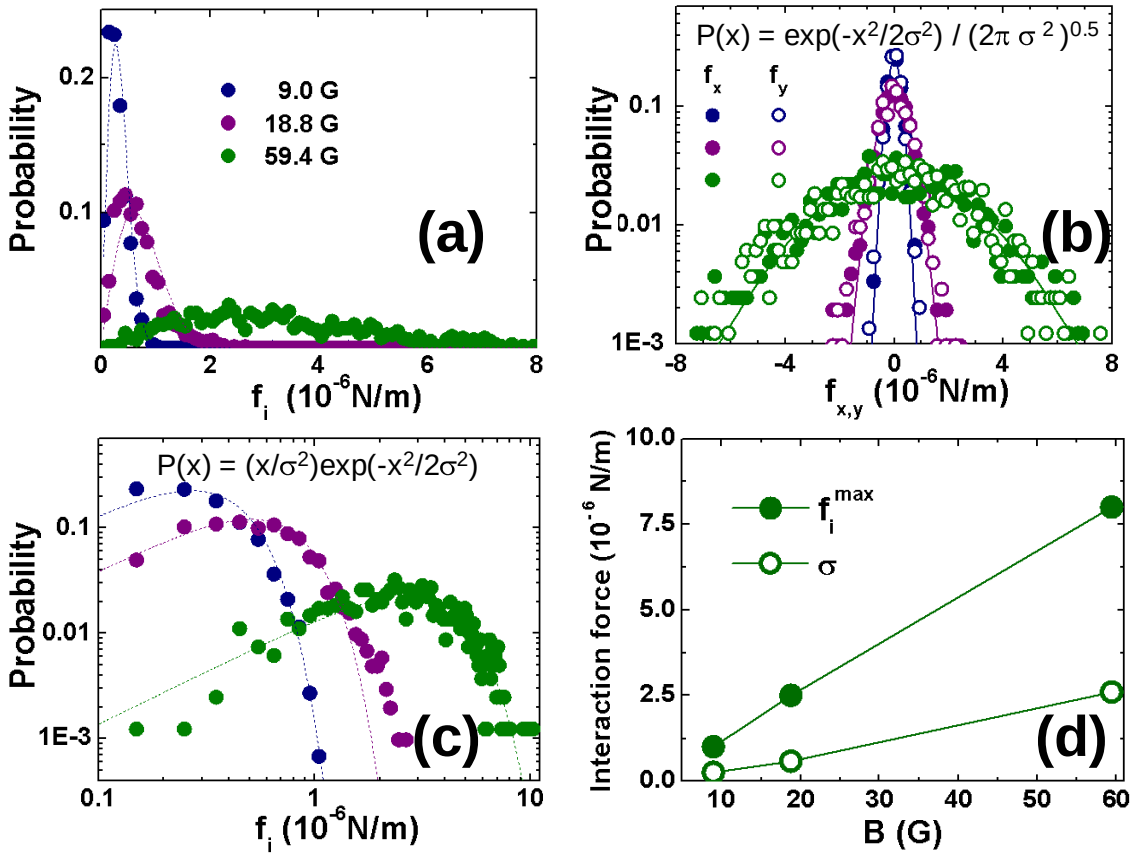

Figure 6: Distributions of the inter-vortex repulsive force per unit length for $Bi_2Sr_2CaCu_2O_8$ samples with a dense distribution of CD at different vortex densities. (a) Modulus of the inter-vortex force (points) and fits to the data with Rayleigh functions (dotted lines). (b) Distributions of the x-(full points) and y-(open points) components of the inter-vortex force and fits with a symmetric Gaussian distribution (full lines). (c) Same distributions as in (a) plotted in log-log scale and fits to the data with Rayleigh functions (dotted lines). (c) Standard deviation and maximum values of the inter-vortex force modulus distributions as a function of vortex density.

by a vortex, and $n_k = 0$ otherwise. In each metastable state the interaction force f_i must balance in average the defect-vortex force on vortex i. During the lifetime of the metastable state, controlled by thermal activation, vortices are bound to their columnar defects, only performing small futile fluctuations. Near freezing, the lifetime of metastable states are expected to be comparable to experimental times, and their typical configurations similar to the ones observed by magnetic decoration. We are thus considering that cooling down to 4.2 K for magnetic decoration has only the effect of further stabilizing the metastable configuration frozen at T_freez. We will use this criterion for inferring information about the dynamics near the freezing of the observed vortex structures.

In order to model the non-stationary dynamics connecting different metastable states after a temperature quench, we will assume that the relaxation process is mainly dominated by single vortex hopping between the randomly-distributed CD. We are thus neglecting multiple vortex hopping, which might be important at higher vortex densities. For simplicity, we will consider identical CD, the so-called non-dispersive case.[1] Under this assumption, the contribution of super-kink excitations is not considered and thus the optimal thermal excitations of an individual vortex line are either half-loops or double kinks (DK).[1] These excitations allow a vortex to escape from one columnar defect, and to be then retrapped by a nearby defect located at a typical distance $d \sim (\Phi_0/B_\Phi)^{1/2} \ll a_0$. Since we also have $d \ll \lambda_\mathrm{ab}(0) < \lambda_\mathrm{ab}(T)$, the vortex-defect force on vortex i is practically the same for consecutive metastable states. If we denote the metastable state at a given time by a supraindex α, the relaxation process connecting different metastable states can thus be effectively viewed as a non-steady transport process driven by the heterogeneous set of average local forces associated to the metastable state, $\{\mathbf{f}_\mathrm{i}^\alpha\}$. The dependence of f_i with α allow us to effectively include the non-steady variation of vortex-vortex interactions during the relaxation and its magnetic field dependence.

Half-loops excitations are expected to be relevant for pinned vortices such that $f_\mathrm{d} < f_i^\alpha < f_\mathrm{c}$, where $f_\mathrm{d} \approx U_0/d$

is the force at which a half-loop involves a displacement of the order of the average separation between defects, d, and $f_c \approx U_0/r_r$ is the critical depinning force from a single defect. As we show below, half-loops drive the relaxation at very short time-scales; for larger times most local forces f_i^α drop below f_d and half-loop excitations are exhausted. Therefore, at large time-scales relaxation is mainly driven by DK excitations since most of vortices feel an interaction force $f_i < f_d$ from the other vortices. Optimal DK have a longitudinal length $z \approx d\sqrt{\epsilon_l/U_0}$ and cost an energy $2E_K \approx 2d\sqrt{\epsilon_l U_0}$. The line tension $\epsilon_l \sim \varepsilon_0/\Gamma^2$ is normalized by the anisotropy of the vortex system Γ, and corresponds to the limit of short-wavelength distortions in the c direction involved in the kink formation. The proliferation of optimal DK excitations allow a vortex localized at a defect to hop to a neighbor one at a distance of the order of d. Provided that the energy barrier for such excitation, $U_i^\alpha = (2E_K - f_i^\alpha dz)$, is larger than $k_B T$, the typical time to escape from the defect is given by the Arrhenius law $\tau_i^\alpha = \tau_0 e^{U_i/k_B T}$, yielding

$$\tau_i^\alpha \approx \tau_0\, e^{(2d\sqrt{\epsilon_l U_0} - d^2\sqrt{\epsilon_l/U_0} f_i^\alpha)/k_B T}, \qquad (3)$$

where τ_0 is a characteristic time, or inverse of the attempt frequency. The last formula is an estimate for the *escape time* of a vortex i feeling the force f_i^α coming from its interaction with all other vortices *on a given metastable state* α.

We can define the lifetime of a given metastable configuration α just as the minimum single-vortex escape-time among all vortices, as one vortex hop changes a pair of CD occupation numbers, producing a new metastable state α'. Such a minimal escape time corresponds to the minimal escape barrier $U^\alpha = \min_i[2d\sqrt{\epsilon_l U_0} - d^2\sqrt{\epsilon_l/U_0} f_i^\alpha]$. Therefore, it corresponds to the escape time of the least bounded vortex, feeling the maximum force $f_{\max}^\alpha = \max_i[f_i^\alpha]$ in the metastable configuration α. Remembering that $U_0 \sim \varepsilon_0(r_r^2/2\xi^2)$, we finally get the scape-time for a given metastable configuration

$$\tau^\alpha \approx \tau_0 \exp\left[\frac{U^\alpha(a_0, \lambda_{ab}, d, r_r)}{k_B T}\right], \qquad (4)$$

where we have defined the effective energy barrier associated with a given pinned configuration α,

$$U^\alpha \equiv U^\alpha(a_0, \lambda_{ab}, d, r_r) = \left(1 - \frac{\tilde{f}_{max}^\alpha(a_0, \lambda_{ab}) d\lambda_{ab}}{2\kappa^2 r_r^2}\right) 2E_K, \qquad (5)$$

as a function of the characteristic lengths a_0, λ_{ab}, d and r_r. The dimensionless force $\tilde{f}_{\max}^\alpha = f_{\max}^\alpha 2\lambda_{ab}/\varepsilon_0$, is defined as

$$\tilde{f}_{\max}^\alpha(a_0, \lambda_{ab}) = \max_i \left| \sum_{j \neq i} K_1(\mathbf{r}_{ij}/\lambda_{ab}) \frac{\mathbf{r}_{ij}}{r_{ij}} \right|, \qquad (6)$$

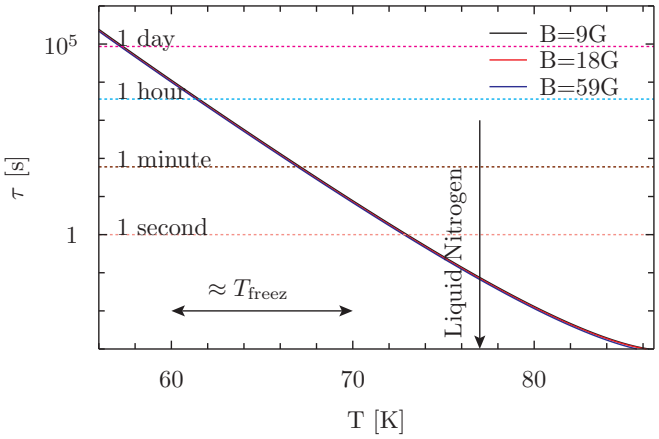

Figure 7: Lifetime of the decorated metastable vortex configuration vs. temperature, assuming only double-kink excitations during the relaxation of metastable states. We indicate the estimated freezing temperature T_{freez} at which the vortex structure is frozen at lengthscales of a_0 as revealed by magnetic decoration.

and can be directly obtained from the magnetic decoration images with α corresponding to the frozen metastable state. The DK energy-cost can be written in terms of the characteristic lengths λ_{ab}, d, and r_r as

$$2E_K \equiv 2E_K(\lambda_{ab}, d, r_r, \Gamma, \kappa) = \sqrt{2}\frac{\kappa r_r d\varepsilon_0}{\lambda_{ab}\Gamma}. \qquad (7)$$

Within this model, the field-dependence of the lifetime is thus completely absorbed in the maximum value of the defect-vortex force distribution for the given frozen configuration $f_{\max}^\alpha$.

Let us first start estimating the lifetime τ of the decorated metastable vortex configurations —we will drop the supraindex α when referring to the frozen metastable state— by making again the reasonable assumption that they were frozen at, or very near to, the irreversibility line, namely $T_{freez} \approx T_{irr}$. From expressions of equations

B [G]	$\lambda_{ab}(T_{irr})[\mu m]$	$T_{irr}[K]$	$\tilde{f}_{\max}(\lambda_{ab}(T_{irr}))$	$U/k_B[K]$	$\tau[s]$
9	0.69	85.3	0.6	25	0.0013
18.8	0.59	83.9	0.93	40	0.0016
59.4	0.39	79.6	1.3	137	0.0056

Table I: Estimate of the lifetime τ of the magnetically decorated metastable vortex configurations frozen during field-cooling at $T = T_{irr}$ by assuming only DK excitations. We have used the following experimental parameters: $d = 0.065\ 10^{-4} cm$, $r_r = 3.5\ 10^{-7} cm$, $(d/r_r \sim 20)$, $\lambda(T=0) = 0.18\ 10^{-4} cm$, $T_c = 86.7$ K, $\kappa \approx 200$, $\Gamma \approx 150$. The parameters $\lambda_{irr} = \lambda(T_{irr})$ and $\epsilon_0^{irr} = (\Phi_0/4\pi\lambda_{irr})^2$. The value $\tau_0 \sim 10^{-3} s$ is taken from the measured frequency-dependent ac creep response in the half-loop regime in the same sample reported in Ref. 53.

(4), (5), (6), and (7), we get the results for $\tilde{f}^{\alpha}_{\max}$ and τ shown in Table I, where the value of the experimental parameters for these samples are indicated in the caption. In all cases we verified that $\tilde{f}_d(\lambda_{\rm irr}) > \tilde{f}_{\max}(\lambda_{\rm irr})$ so that half-loop excitations are not relevant. The estimated lifetimes of Table I, of the order of $\tau_0 \sim 10^{-3}\,$s, are much smaller than the typical time-scales of decoration experiments, namely $\tau(T_{\rm irr}) \ll \tau_{\rm exp}$, with $\tau_{\rm exp}$ of the order of seconds or minutes. Therefore, we should necessarily have $T_{\rm freez} < T_{\rm irr}$ since the freezing temperature should correspond to $\tau(T_{\rm freez}) \sim \tau_{\rm exp}$. Forcing such a condition, from equations (4), (5), (6), and (7) we can estimate the value of $T_{\rm freez}$. In order to do this realistically, we need to know the temperature-dependence of $\lambda_{\rm ab}$ at $T < T_{\rm irr}$. Here, we will simply assume the dependence $\lambda_{\rm ab}(T) = \lambda_{\rm ab}(0)/\sqrt{1-(T/T_{\rm c})^4}$ with $\lambda_{\rm ab}(0) = 180\,$nm. This dependence yields a very reasonable analytical approximation for the values measured at $T \sim T_{\rm irr}$ in Ref. 22 and shown in Table I for $T = T_{\rm irr}(B)$ for the studied vortex densities.

Recalculating $\tilde{f}^{\alpha}_{\max}$ and U^{α} as a function of T using this approximation for $\lambda_{\rm ab}(T)$, and setting $\tau(T_{\rm freez}) \sim \tau_{\rm exp}$, with $\tau_{\rm exp}$ ranging from seconds to hours, we get freezing temperatures in the range $T_{\rm freez} \approx 60 - 70K$ as shown in Fig. 7. As we can see from this figure, the field-dependence of the lifetimes, and thus $\tau(T_{\rm freez})$, is very weak. It is also interesting to note that at the liquid nitrogen temperature, at which the superconducting sample spends some minutes during the cooling protocol down to 4.2 K, the dynamics is relatively fast, with lifetimes of the order of milliseconds. This means that the frozen configuration should have a memory of a lower temperature, $T_{\rm freez}$, indicated in Fig. 7.

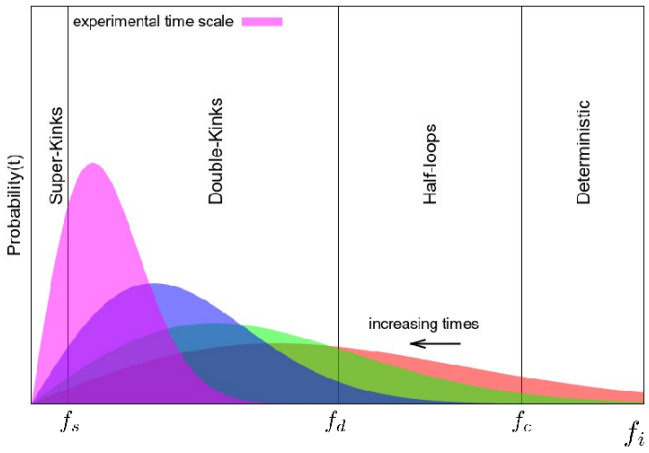

Figure 8: Schematic picture for the distribution of the local force relaxation process, in the limit $d \ll a_0, \lambda_{\rm ab}$. The system starts from a highly disordered state with a broad distribution of local forces. As relaxation goes on, the force distribution becomes narrower, and the system gets quickly trapped in metastable states when all forces lie below $f_{\rm c}$. Thermally activated optimal hops then allow vortices to escape from their columnar defects via different mechanisms: half-loops for $f_{\rm d} < f < f_{\rm c}$, double-kinks for $f_{\rm s} < f < f_{\rm d}$, and super-kinks for $f < f_{\rm s}$ (for identical columnar defects $f_{\rm s} = 0$), where $f_{\rm c}$, $f_{\rm d}$ depend on the pinning energy, radius and separation between columnar defects and $f_{\rm s}$ also depends on the degree of columnar disorder. During a field-cooling process, the distribution becomes practically frozen (thicker curve) for the experimental time scale at some characteristic temperature $T_{\rm freez}$

V. DISCUSSION

The predictions from the model discussed in the previous section suggest that the decorated configurations are far from the equilibrium configuration at 4.2 K and that are dynamically frozen at $T_{\rm freez}$ by the strong decrease of vortex mobility with temperature induced by the CD dense pinning potential. Within the model, this mobility is dominated by Arrhenius activation through the temperature-dependent *finite* barriers associated with DK excitations, as barriers for half-loops can be overcame in typical times of the order of milliseconds and the larger barriers expected for super-kinks were disregarded on the basis that DK alone are able to yield metastable states with macroscopic lifetimes. Within this scenario, it is worth mentioning that previous works studying samples with $B_\Phi = 5\,$kG from the same batch than ours reported[53] that the low-field regime presented non-divergent activation barriers varying linearly with the ac driving current. This is in contrast to the divergent barriers found at higher fields, consistent with half-loop excitations. On the other hand, it was proposed that for a high density of CD the changes in pinning energies when increasing field are negligible compared to the change in interaction energy, giving place to a "discrete superconductor" picture.[50] These two findings are consistent with our model assumption that the relevant excitations driving the non-steady relaxation are just DK and that the role of super-kink excitations is not important for the time-scales we aim to describe. Note that this is in contrast with the barriers expected for a glass, which tend to diverge near equilibrium, a signature of the localization of vortex lines at very long times. The amorphous order observed in the decorations can then be interpreted as a snapshot of a non-entangled liquid-like structure metastable at $T_{\rm freez}$, a temperature located below the first-order transition line. This non-entangled highly viscous and *far from equilibrium* liquid-like structure contrasts with the quasi-long-range positionally-ordered vortex structures observed in pristine samples of the same compound at $T < T_{\rm FOT}$.[10]

Figure 8 shows a schematic picture for the relaxation dynamics of the defect-vortex forces. Within our model, the dynamics at $T_{\rm freez}$ is mainly controlled by DK excitations since most of the defect-vortex forces satisfy $f_{\rm s} < f < f_{\rm d}$, with $f_{\rm s} \sim \gamma/d$ the force below which super-kink excitations dominates. The parameter γ is

the dispersion in pinning energies coming from the differences between columnar defects and from the disorder in their spatial distribution. In our model we have assumed, for simplicity, that γ is negligible compared to U_0, so f_s is very small and super-kink dynamics would become relevant only at very large time-scales. If γ is not small, then the non-steady relaxation may be dominated by variable range hopping hops with DK becoming inefficient to irreversibly drive the vortices to a lower energy state.

A previous work[50] proposes that the low-field vortex state nucleated in the case of a sample with a dense distribution of CD would not differ fundamentally from that observed in pristine samples. This is based in the finding that the energy difference between two metastable states in the former case is dominated by the vortex-vortex interaction energy rather than by the differences in pinning energy. Within this proposal, each vortex line is however confined and pinned to a CD. This proposal is similar to the one stating that the conventional Bose glass phase may have a crossover to a putative "Bragg-Bose glass phase"[54]. The later is a glassy phase with quasi-long-range order but confined in CD, and thus individual vortex lines are macroscopically flat, in sharp contrast to the rough vortex lines of the Bragg-glass phase expected for weak point-disorder. Interestingly, our analysis suggests that the truly glassy relaxation dynamics in our samples, such as the super-kink or variable range hopping dynamics, or collective creep dynamics made of correlated hops, corresponding to one of the possible equilibrium phases, would become dominant only in the limit of very long relaxation times, *much larger* than the one probed during the magnetic decoration quenching process. These experiments, as they are currently done, can not give any information about the subjacent equilibrium glass phase expected at very long-times. We believe this will critically depend on the degree of dispersion of the pinning energies, $\gamma \sim f_s d$,[1].

Therefore, it would be interesting to implement glass-annealing techniques in order to reach configurations with a narrower distribution of vortex-defect forces and thus with less memory of the liquid phase and less accumulated stress. Observing the changes in the translational order of the decorated lattice as a function of the quenching time, for instance, may tell us which phase is more plausible, as the corresponding equilibrium correlation length slowly grows with time. In particular, if a topologically ordered equilibrium phase exists at low fields in the presence of a high density of CD or a "discrete superconductor" picture is valid, then the density of dislocations in the vortex structure should display a decrease with time. This effect might be seen, for instance, by comparing the number of $\rho_{\rm def}$ detected in magnetic decoration experiments performed at very different cooling rates.

VI. CONCLUSIONS

We have analyzed, through magnetic decoration images, dynamically frozen vortex configurations in heavy-ion irradiated $Bi_2Sr_2CaCu_2O_8$ samples with a very dense distribution of columnar defects. For low vortex densities compared with the CD density, we find an amorphous phase with liquid-like correlations, and an approximately Gaussian defect-vortex force distribution indicating a randomly-oriented pinning scenario. By assuming vortices individually trapped at identical CD, we show that the observed translational order is fairly consistent with a relaxation dynamics dominated by DK excitations near the freezing temperature $T_{\rm freez}$. Using a simple model we predict a freezing temperature of the same order but smaller than the irreversibility temperature, the temperature at which bulk pinning becomes dominant, detected as the onset of non-linear magnetic response at low frequencies. We argue that magnetically-decorated structures hence correspond to a typical configuration of a non-entangled vortex-liquid state with a strongly reduced mobility, rather than a typical metastable state of a subjacent equilibrium glassy phase.

VII. ACKNOWLEDGMENTS

This work was made possible thanks to the support of the ECOS-Sud-MinCyT France-Argentina bilateral program, Grant No. A09E03. Work done at Bariloche was partially founded by PICT-PRH 2008-294 and University of Cuyo Reserch Grant No. 06-C381. A.B.K, D.D. and Y.F. also acknowledge support from ANPCyT-PICT-2011-1537.

[1] G. Blatter, M. V. Feigel'man, V. B. Geshkenbein, A. I. Larkin, and V. M. Vinokur, Rev. Mod. Phys. **66** 1125 (1994).
[2] Y. Fasano, and M. Menghini, Supercond. Sc. and Tech. **21**, 023001 (2008).
[3] M. N. Grisolia, C. J. van der Beek, Y. Fasano, A. Forget, D. Colson, Phys. Rev. B **87** 104517 (2013).
[4] G. Grüner, Rev. Mod. Phys. **60** 1129 (1988).
[5] J. Gorchon, S. Bustingorry, J. Ferré, V. Jeudy, A. B. Kolton, and T. Giamarchi, Phys. Rev. Lett. **113** 027205 (2014).
[6] K.-J. Kim et al., Nature **458**, 740 (2009).
[7] P. Paruch and J. Guyonnet, C. R. Physique **14** 667 (2013).
[8] J. F. Joanny, P.-G. de Gennes, A model for contact angle h ysteresis, J. Chem. Phys. **81** 552 (1984); S. Moulinet and A. Rosso and W. Krauth and E. Rolley, Phys. Rev. E **69** 035103(R) (2004).
[9] M. Alava, P. K. V. V. Nukalaz, S. Zapperi, Statistical models of fracture, Adv. Phys. **55** 349 (2006); L. Ponson, Phys. Rev. Lett. **103**, 055501 (2009).

[10] Y. Fasano, M. De Seta, M. Menghini, H. Pastoriza, and F. de la Cruz, Proceed. Nat. Acad. Sciences **102**, 3898 (2005), and references therein.

[11] A. P. Petrovic, Y. Fasano, R. Lortz, C. Senatore, A. Demuer, A.B. Antunes, A. Paré, D. Salloum, P. Gougeon, M. Potel, Ø. Fischer, Phys. Rev. Lett. **103** 257001 (2009).

[12] Y. Fasano, J. Herbsommer, and F. de la Cruz, Phys. Stat. Sol. (b) **215** 563 (1999).

[13] Y. Fasano, M. De Seta, M. Menghini, H. Pastoriza, and F. De la Cruz, Solid State Comm.**128** 51 (2003).

[14] S. Demirdis, C. J. van der Beek, Y. Fasano, N. R. Cejas Bolecek, H. Pastoriza, D. Colson, and F. Rullier-Albenque, Phys. Rev. B **84**, 094517 (2011).

[15] C.J. van Der Beek, S. Demirdis, M. Konczykowski, Y. Fasano, N. R. Cejas Bolecek, H. Pastoriza, D. Colson, and F. Rullier-Albenque, Phys. B: Condensed Matter **407** 1746 (2012).

[16] S. Demirdis, Y. Fasano, S. Kasahara, T. Terashima, T. Shibauchi, Y. Matsuda, M. Konczykowski, H. Pastoriza, C.J. van der Beek, Phys. Rev. B **87** 094506 (2013).

[17] H. Yang, B. Shen, Z. Wang, L. Shan, C. Ren, and H.-H. Wen, Phys. Rev. B **85**, 014524 (2012).

[18] C.J. van der Beek, S. Demirdis, M. Konczykowski, Y. Fasano, N.R. Cejas Bolecek, H. Pastoriza, D. Colson, F. Rullier-Albenque, Phys. B **407**, 1746 (2012).

[19] C. J. van Der Beek, S. Demirdis, D. Colson, F. Rullier-Albenque, Y. Fasano, T. Shibauchi, Y. Matsuda, S. Kasahara, P. Gierlowski, M. Konczykowski, J. Phys. Conf. Series **449**, 012023 (2013).

[20] L. Civale, A.D. Marwick, M.W. McElfresh, T.K. Worthington, A. P. Malozemoff, F. H. Holtzberg, J. R. Thompson, and M. A. Kirk, Phys.Rev.Lett. **65** , 1164 (1990).

[21] M. Konczykowski, F. Rullier-Albenque, E. R. Yacoby, A. Shaulov, Y. Yeshurun, and P. Lejay, Phys. Rev. B **44** , 7167 (1991).

[22] C. J. van der Beek, *Thermodynamique des vortex dans les supraconducteurs desordonnes*, Südwestdeutscher Verlag für Hochschulschriften AG & Co. KG, Sarrebruck, Germany (2010).

[23] G. S. Mkrtchyan, and V. V. Shmidt, Zh. Eksp. Teor. Fiz. **61**, 367 (1971). [Sov. Phys. JETP **34**, 195 (1972)].

[24] D. R. Nelson, V. M. Vinokur, Phys. Rev. B **48** 13060 (1993).

[25] A. Buzdin, D. Feinberg, Phys. C **235-240** 2755 (1994).

[26] N. Takezawa, K. Fukushima, Phys. C **228** 149 (1994).

[27] R. J. Drost, C. J. van der Beek, H. W. Zandbergen, M. Konczykowski, A. A. Menovsky, and P. H. Kes, Phys. Rev. B **59**, 13612 (1999).

[28] A. Wahl, V. Hardy, J. Provost, Ch. Simon, A. Buzdin, Phys. C **250** 163 (1995).

[29] U. C. Tauber, H. Dai, D. R. Nelson, and Ch. M. Lieber Phys. Rev. Lett. **74** 5132 (1995).

[30] M. Leghissa, L. A. Gurevich, M. Kraus, G. Saemann-Ischenko, L. Ya. Vinnikov, Phys. Rev. B **48**, 1341 (1993).

[31] H. Dai, S. Yoon, J. Liu, R. C. Budhani, Ch. M. Lieber, Science **265**, 1552 (1994)

[32] M. Menghini, Yanina Fasano, F. de la Cruz, S. S. Banerjee, Y. Myasoedov, E. Zeldov, C. J. van der Beek, M. Konczykowski and T. Tamegai, Phys. Rev. Lett. **90** , 147001 (2003).

[33] S. S. Banerjee, A. Soibel, Y. Myasoedov, M. Rappaport, E. Zeldov, M. Menghini, Yanina Fasano, F. de la Cruz, C. J. van der Beek, M. Konczykowski and T. Tamegai, Phys. Rev. Lett. **90** , 087004 (2003).

[34] M. Menghini, Yanina Fasano, F. de la Cruz, S.S. Banerjee, Y. Myasoedov, E. Zeldov, C. J. van der Beek, M. Konczykowski and T. Tamegai, J. Low Temp. Phys. **135** , 139 (2004).

[35] S. S. Banerjee, A. Soibel, Y. Myasoedov, M. Rappaport, E. Zeldov, M. Menghini, Yanina Fasano, F. de la Cruz, C. J. van der Beek, M. Konczykowski and T. Tamegai, Phys. C **408-410** , 495 (2004).

[36] Yanina Fasano, M. De Seta, M. Menghini, H. Pastoriza and F. de la Cruz, Phys. C **408-410** , 520 (2004).

[37] M. Menghini, Yanina Fasano, F. de la Cruz, S. S. Banerjee, Y. Myasoedov, E. Zeldov, C. J. van der Beek, M. Konczykowski and T. Tamegai, on *Perspectives on Superconductivity Research*, edited by P.S. Lewis , Nova Publishers (2005).

[38] F. Pardo, A. P. Mackenzie, F. de la Cruz, and J. Guimpel, Phys. Rev. B **55**, 14610 (1997).

[39] T. W. Li *et al.*, J. Cryst. Growth **135**, 481 (1994).

[40] A. Dorosinskii, M. V. Indenbom, V. I. Nikitenko, Yu A. Ossip'yan, A. A. Polyanskii, and V. K. Vlasko-Vlasov, Physica C **203**, 149 (1992).

[41] M. Konczykowski, F. Holtzberg, and P. Lejay, Supercond. Sci. Technol. **4**, S331 (1991).

[42] H. Pastoriza, M. F. Goffman, A. Arribere, and F. de la Cruz, Phys. Rev. Lett. **72**, 2951 (1994).

[43] E. Zeldov, D. Majer, M. Konczykowski, V. B. Geshkenbein, V. M. Vinokur, and H. Shtrikman, Nature **375**, 373 (1995).

[44] M. Konczykowski, C. J. van der Beek, A. E. Koshelev, V. Mosser, M. Dogson, and P. H. Kes, Phys. Rev. Lett. **97**, 237005 (2006).

[45] J. Gilchrist, and M. Konczykowski, Phys. C **212**, 43 (1993).

[46] H. Pastoriza and P. H. Kes, Phys. Rev. Lett. **75**, 3525 (1995).

[47] N. Morozov, E. Zeldov, D. Majer, and M. Konczykowski, Phys. Rev. B **54**, R3784 (1996).

[48] M. I. Dolz, Y. Fasano, H. Pastoriza, V. Mosser, M. Li, M. Konczykowski, Phys. Rev. B, **90** 144507 (2014).

[49] C. J. van der Beek, M. Konczykowski, R. J. Drost, P. H. Kes, N. Chikumoto, and S. Bouffard, Phys. Rev. B **61**, 4259 (2000).

[50] C. J. van der Beek, M. Konczykowski, A. V. Samoilov, N. Chikumoto, S. Bouffard, and M. V. Feigel'man, Phys. Rev. Lett. **86**, 5136 (2001).

[51] M. V. Indenbom, C. J. van der Beek, V. Berseth, M. Konczykowski, N. Motohira, H. Berger, W. Benoit, J. Low Temp. Phys. **105**, 1117 (1996).

[52] N. R. Cejas Bolecek, M. I. Dolz, A. Kolton, H. Pastoriza, C. J. van der Beek, M. Konczykowski, M. Menghini, G. Nieva, Y. Fasano, J. Low Temp. Phys. **179** 35 (2015).

[53] C. J. van der Beek, M. Konczykowski, V. M. Vinokur, T. W. Li, P. H. Kes, and G. W. Crabtree Phys. Rev. Lett. **74**, 1214 (1995); C. J. van der Beek, M. Konczykowski, V. M. Vinokur, G. W. Crabtree, T. W. Li, and P. H. Kes Phys. Rev. B **51**, 15492 (1995).

[54] T. Giamarchi and P. Le Doussal, Phys. Rev. B **55**, 6577 (1997).